Solvent-free synthesis of protic ionic liquids. Synthesis, characterization and computational studies of triazolium based ionic liquids

Journal of Molecular Liquids 360 (2022) 119358

Contents lists available at ScienceDirect

Journal of Molecular Liquids

journal homepage: www.elsevier.com/locate/molliq

Solvent-free synthesis of protic ionic liquids. Synthesis, characterization and computational studies of triazolium based ionic liquids

Eduardo Maurina Morais [1], Iqbaal Abdurrokhman [1], Anna Martinelli *

Department of Chemistry and Chemical Engineering, Chalmers University of Technology, 41296 Gothenburg, Sweden

ARTICLE INFO

Article history:
Received 20 July 2021
Revised 6 April 2022
Accepted 7 May 2022
Available online 14 May 2022

Keywords:
Protic Ionic Liquid
Solvent-free
Synthesis
DFT
Vibrational Assignment
Acidity

ABSTRACT

A series of triazolium and imidazolium based protic ionic liquids were synthesized using a solvent-free method designed to address several limitations encountered with other commonly used methods. Using this method, pure (98–99% m/m) and dry (128–553 ppm of water) protic ionic liquids were synthesized (in a laboratory scale) without the need for purification methods that require heating the ionic liquid, hence avoiding the common issue of thermal decomposition. This method was also designed to allow for the accurate measurement of acid and base, and for the controlled mixing of both compounds, which is essential to avoid producing impure protic ionic liquids with excess of either acid or base. The system is constructed of only glass and chemically resistant polymer (PTFE and PVDF) parts, which avoid other contaminants that can result from unwanted reactions involving the reagents with common laboratory tools (metallic objects, paper, plastic, *etc.*). This process is described in detail in the paper as well as in a video. The resulting ionic liquids were carefully analyzed by spectroscopic and thermal methods designed to avoid water absorption, which is known to affect their properties. To complement this experimental characterization, computational chemistry tools were used to assess the ionic liquids' properties, as well as to assign vibrational modes.

1. Introduction

Protic ionic liquids are a sub-category of the broader ionic liquid category of compounds, with the distinctive feature of being the result of a neutralization reaction between an acid and a base. These protic ionic compounds have a melting point lower than 100 °C, at times even lower than room temperature. Due to their unique properties, they are relevant for a variety of applications, most notably as electrolytes for fuel cells and, specifically, in proton exchange membranes [1,2]. The interest in protic ionic liquids has steadily grown, as evidenced by the increasing number of publications in the field. This, combined with a limited commercial availability, induces many research groups to synthesize their own protic ionic liquids of interest. Moreover, given the theoretical simplicity of the synthesis, these compounds appeal even to research groups with little experience in the synthesis of ionic liquids. Unfortunately, many works dealing with the preparation of these compounds report narrow descriptions of the experimental procedure, which is sometimes limited to be a 'mixing of the acid and the base at an equimolar ratio'. With this oversimplification a series of concerns risk to be overlooked, which certainly should be addressed when aiming at pure protic ionic liquids; like avoiding water absorption, keeping the mole ratio of acid to base as close as possible to unity (avoiding the excess of unreacted acid or base), reducing contamination or avoiding thermal decomposition. These concerns should also be at focus during the analysis and characterization procedures, such that these do not cause significant property changes during the investigation.

The core objective of this work was obtaining a series of triazolium and imidazolium protic ionic liquids with a high level of purity *via* a clean solvent-free synthesis. Also, the thermal (experimental) and spectroscopic (experimental and computational) properties of these ionic liquids were characterized, with the aim to determine their applicability as proton conducting compounds in proton exchange membrane fuel cells (the transport properties of these compounds will be reported in a separate and subsequent publication). This work is written in a way that many experimental and computational details are provided and discussed, for the dual sake of accuracy and reproducibility (a video showing all the experimental steps is also included, serving as a visual complement to the already comprehensive text). Two well known anions are considered, *i.e.*, triflate (TfO) and bistriflimide (TFSI), while the cations were selected to be the 1-ethylimidazolium (relatively well known and studied, hence useful as a benchmark for results) and

* Corresponding author.
E-mail address: anna.martinelli@chalmers.se (A. Martinelli).
[1] These authors contributed equally to this work.

https://doi.org/10.1016/j.molliq.2022.119358
0167-7322/

1-ethyl-1,2,4-triazolium that is an emerging cation in the field of protic ionic liquids [3,4] (Fig. 1).

We sincerely hope that, given the level of details provided, this work will serve as a stepping stone for other researchers to further develop methodologies for the careful synthesis and characterization of clean protic ionic liquids.

2. Experimental

2.1. Materials

Iodoethane (copper stabilized) 99%, 1,2,4-triazole 98%, anhydrous potassium carbonate, Celite® 545 (treated with sodium carbonate, flux calcined), activated charcoal (powder, 100 mesh) and 0.6 mL ampules of DMSO-d_6 99.9% D with 0.03% TMS (v/v) were purchased from Sigma Aldrich, stored in a regular chemical storage cabinet and used without any purification or special preparation. Trifluoromethanesulfonic acid (25 g ampule) 99.6% (assay by NaOH titration by the manufacturer - LOT MKCM2349) and Trifluoromethanesulfonimide 99.5% (assay by ^{19}F-qNMR - described in the experimental section) were purchased from Sigma Aldrich, stored inside of a N_2 filled MBRAUN UNIlab Plus Eco glovebox with a MB-LMF II solvent absorber system and used without any purification or special preparation. 1-Ethylimidazole 99.4% (assay by GC by the manufacturer - LOT S7377630944) was purchased from Merck, stored inside a glovebox and used without any purification or special preparation. 4-Fluoroacetophenone 99.8% (assay by GC by the manufacturer - LOT A0372446) was purchased from Acros Organics, stored in a regular chemical storage cabinet and used without any purification or special preparation. Hydranal™ Coulomat AD was purchased from Fluka, stored in a regular chemical storage cabinet and used without any purification or special preparation. Molecular sieves 3Å (4–8 mesh) were purchased from Sigma Aldrich, dried in a vacuum oven at 180 °C overnight and under full vacuum, and then stored in a glovebox. 1-Ethylimidazolium triflate 99.7% (assay by ^{19}F-qNMR - described in the experimental section) was purchased from IoLiTec, stored inside a glovebox and used without any purification or specific preparation. Acetone and acetonitrile (HPLC grade) were purchased from various suppliers and used without any purification or special preparation. Syringe filters with PTFE membranes (0.2 μm pore size) from FisherBrand were purchased from Fisher Scientific.

2.2. Synthesis

2.2.1. Synthesis of the base

1-Ethyl-1,2,4-triazole was synthesized using a modified procedure based on the one described by Alpers et al. [5] A mixture of 1,2,4-triazole (40 g, 0.579 mol, 1 equiv), K_2CO_3 (160.1 g, 1.158 mol, 2 equiv) and acetone (200 mL) was added to a 500 mL 3-necked round bottom flask adapted with a water cooled condenser, a glass cap and a dropping funnel filled with iodoethane (108.4 g, 0.695 mol, 1.2 equiv). The iodoethane was added dropwise to the reaction mixture, which was cooled with an ice bath and stirred with a magnetic stirrer. After the addition of the iodoethane, the dropping funnel was substituted by a glass stopper and the solution was heated up to 60 °C for 24 h in an oil bath. After completion, the solids were removed by filtration and most of the solvent was removed by using a rotavapor (40 °C at 25 kPa). The crude product was purified using a Kugelrohr short-path vacuum distillation apparatus (Büchi B-585) at 95 °C and 1 kPa. The product was then redistilled, resulting in a colorless and clear liquid. Activated charcoal and molecular sieves were added to the product to remove impurities and to reduce the water content. 24 h later, the molecular sieves were decanted and the mixture was filtered through a PTFE syringe filter to remove the remaining activated charcoal. The 1-ethyl-1,2,4-triazole 98.8% (assay by GC) was obtained as a colorless and clear liquid, furthermore, it was kept inside a glovebox and mixed with fresh molecular sieves. ^{1}H-NMR (400 MHz, DMSO-d_6, referenced with 0.03 % v/v TMS in DMSO-d_6) = δ 8.52 (s, 1H), 7.96 (s, 1H), 4.20 (m, 2H), 1.39 (t, 3H). ^{13}C-NMR (101 MHz, DMSO-d_6, referenced with DMSO-d_6) = δ 151.23, 143.28, 43.74, 14.97.

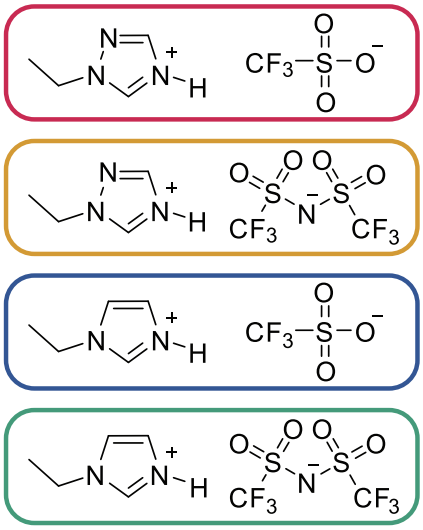

Fig. 1. Molecular structure and color coding of all the protic ionic liquids considered in this study. From top to bottom: [C_2HTr_{124}][TfO], [C_2HTr_{124}][TFSI], [C_2HIm][TfO] and [C_2HIm][TFSI].

2.2.2. Synthesis of the ionic liquids

The three ionic liquids were prepared in the same way ([C_2HTr_{124}][TfO], [C_2HTr_{124}][TFSI] and[C_2HIm][TFSI]). In general, the reaction consists in mixing the two precursors (acid and base) in a mole ratio as close as possible to 1:1, under an inert atmosphere to avoid the absorption of atmospheric water. In order to achieve this precision, a special synthesis setup was developed (Fig. 2). Further details on the motivation for developing and realizing this unique setup can be found in the results and discussion section further down. A video displaying the whole synthesis process is available in the supporting information.

The synthesis setup was dried in a vacuum oven and placed inside the glovebox. The acid was weighed inside the Schlenk vial (containing a PTFE coated magnetic stir bar) using a precision balance that was internally calibrated and checked with a 100 mg reference weight before every use. The base was weighed inside the syringe (already attached to the PTFE tube by a PVDF adapter) using the same balance calibration procedure as the one just described. Both acids, trifluoromethanesulfonic acid (HTfO) and trifluoromethanesulfonimide (HTFSI), were only manipulated using glassware (glass spatula and glass pipettes), to avoid metal contamination due to acid corrosion. In order to achieve an acid to base mole ratio as close as possible to 1:1, the mass of the weighed precursors was corrected using their purity assay values (detailed description of the weighing procedures in the supporting information).

After precisely weighing both precursors, the syringe was attached to the Schlenk vial using a thermometer adapter, making the whole system air-tight. This setup was then quickly removed from the glovebox, attached to a N_2 Schlenk line and kept under a small positive pressure of N_2 to avoid any atmospheric moisture from getting in during the reaction. An ice bath was used to lower

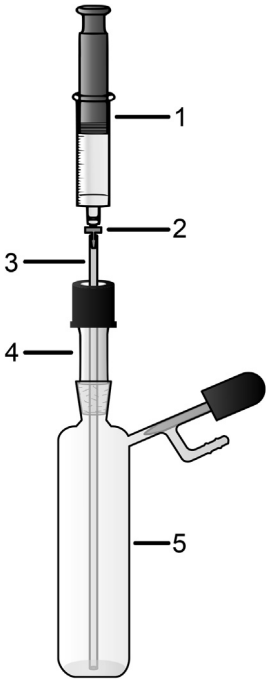

Fig. 2. The setup developed by us and used in this work for the synthesis of the protic ionic liquids. (1) 10 mL gas-tight glass syringe with PTFE plunger seal and male luer lock tip, (2) female luer lock to hose barb PVDF adapter, (3) PTFE tube, (4) thermometer adapter with screw cap and PTFE lined sealing ring, (5) 25 mL Schlenk vial with PTFE screw type needle valve. Detailed information about the commercially available components is present in the supporting information.

the temperature of the contents of the Schlenk vial and a magnetic stirrer was used for mixing. The base was added dropwise to the acid, making sure that the reaction mixture did not overheat and avoiding the risk of side reactions. When all the base had been added, the contents of the Schlenk vial were sucked back into the syringe and then pushed out back into the Schlenk vial several times, to ensure that both precursors mixed fully, without leaving any droplets of unreacted base or acid wetting the walls of the synthesis setup. Afterwards, the whole setup was also shaken to ensure that no droplets of unreacted precursors were left on the walls of the Schlenk vial or the PTFE tube. In the case of a solid forming during the course of the reaction, due to the low temperature of the bath, which would not allow for this recirculation of the reaction mixture, the temperature was increased to 40 °C in order to liquefy the contents of the Schlenk vial (this was, for instance, the case of $[C_2HTr_{124}][TfO]$).

After recirculating the contents of the system, all of the liquid was transferred to the Schlenk vial, the syringe and thermometer adapter were removed and substituted by a glass stopper with PTFE tape, and the contents were allowed to fully react at 40 °C in an oil bath for 1 h. The capped Schlenk vial was then transferred to the glovebox, where dry molecular sieves and activated charcoal were subsequently added to the ionic liquid. After 24 h, the ionic liquid was filtered through a column filled with 1 cm of Celite® 545 and glasswool, to remove most of the solids. Finally, the mixture was filtered through a PTFE syringe filter, resulting in a colorless and clear ionic liquid (it is important to mention that over a period of a few months after the synthesis, the triazolium ionic liquids developed a very faint yellow coloration. This will be further discussed in Section 3.3). The ionic liquids were stored inside the glovebox in clear glass vials with PTFE lined caps. The qualitative NMR spectra of all ionic liquids are reported below, including $[C_2HIm][TfO]$, which was not synthesized and instead purchased from IoLiTec.

$[C_2HTr_{124}][TfO]$: ^{1}H-NMR (700 MHz, neat ionic liquid, referenced with TMS 0.03 % v/v in DMSO-d_6 from capillary) δ 13.59 (s, 1H), 8.92 (s, 1H), 8.13 (s, 1H), 3.83 (q, 2H, J = 7.1 Hz), 0.86 (t, 3H, J = 7.7 Hz). ^{13}C-NMR (176 MHz, neat ionic liquid, referenced with DMSO-d_6 from capillary) δ 142.67, 139.58, 118.12 (q, CF_3, J = 318.6 Hz), 46.11, 12.10. ^{19}F-NMR (659 MHz, neat ionic liquid, no reference) δ −80.22.

$[C_2HTr_{124}][TFSI]$: ^{1}H-NMR (700 MHz, neat ionic liquid, referenced with TMS 0.03 % v/v in DMSO-d_6 from capillary) δ 12.30 (s, 1H), 8.73 (s, 1H), 8.05 (s, 1H), 3.88 (q, 2H, J = 7.4 Hz), 0.96 (t, 3H, J = 7.5 Hz). ^{13}C-NMR (176 MHz, neat ionic liquid, referenced with DMSO-d_6 from capillary) δ 141.83, 138.73, 119.31 (q, CF_3, J = 319.8 Hz), 46.66, 11.75. ^{19}F-NMR (659 MHz, neat ionic liquid, no reference) δ −80.83.

$[C_2HIm][TfO]$: ^{1}H-NMR (700 MHz, neat ionic liquid, referenced with TMS 0.03 % v/v in DMSO-d_6 from capillary) δ 11.97 (s, 1H), 8.13 (s, 1H), 6.89 (s, 1H), 6.80 (s, 1H), 3.62 (q, 2H, J = 7.5 Hz), 0.74 (t, 3H, J = 7.6 Hz). ^{13}C-NMR (176 MHz, neat ionic liquid, referenced with DMSO-d_6 from capillary) δ 133.26, 120.45, 118.51, 118.34 (q, CF_3, J = 319.5 Hz), 43.34, 13.20. ^{19}F-NMR (659 MHz, neat ionic liquid, no reference) δ −80.03.

$[C_2HIm][TFSI]$: ^{1}H-NMR (700 MHz, neat ionic liquid, referenced with TMS 0.03 % v/v in DMSO-d_6 from capillary) δ 11.10 (s, 1H), 7.92 (s, 1H), 6.83 (s, 1H), 6.75 (s, 1H), 3.64 (q, 2H, J = 7.5 Hz), 0.83 (t, 3H, J = 7.6 Hz). ^{13}C-NMR (176 MHz, neat ionic liquid, referenced with DMSO-d_6 from capillary) δ 132.75, 120.46, 119.43 (q, CF_3, J = 320.1 Hz), 118.63, 43.62, 13.00. ^{19}F-NMR (659 MHz, neat ionic liquid, no reference) δ −80.86.

2.3. Characterization

2.3.1. Qualitative analysis

2.3.1.1. Nuclear magnetic resonance spectroscopy (NMR). Qualitative nuclear magnetic resonance of 1-ethyl-1,2,4-triazole was performed using a Varian 400-MR equipped with a OneNMR probe. The sample was prepared by dissolving a small amount of the base in DMSO-d_6 and loading it in a common 5 mm NMR tube. Acquisition of the spectrum was done at 25 °C with spinning at 20 Hz, using the standard pulse sequences and acquisition settings for qualitative ^{1}H and ^{13}C available in the VNMRJ 4.2 software. During the acquisition of the hydrogen spectrum, 120 s of relaxation time was used in order to fully relax the ring hydrogens, which in our experience was more than what is necessary to get the full signal to confirm the 1:1 ratio between peaks. The spectra for the ionic liquids was acquired using a Bruker Avance III 700 MHz equipped with a 5 mm QCI cryoprobe (^{1}H/^{19}F/^{13}C/^{15}N). The samples of pure ionic liquid were loaded in a common 5 mm NMR tube with a coaxial capillary tube filled with DMSO-d_6. All samples were prepared inside the glovebox. Acquisition of the spectrum was done at 25 °C without spinning, using the standard pulse sequences for qualitative ^{1}H (zg30), ^{13}C (zgzrse) and ^{19}F with decoupled ^{1}H (zgig) available on the TOPSPIN 3.6.2 software. The acquisition parameters were 32 scans, 1.75 s acquisition time and 2 s relaxation delay for hydrogen, 64 scans, 0.49 s acquisition time and 0.1 s relaxation delay for carbon and 4 scans, 0.41 s acquisition time and 20 s relaxation delay for fluorine. Spectral analysis was performed using the MestReNova 10.0.0 software. All spectra were baseline and phase corrected. The chemical shifts for hydrogen were referenced using TMS, for carbon using DMSO-d_6, while the fluorine peaks were not reference corrected.

2.3.1.2. Fourier-transform infrared spectroscopy (FTIR). FTIR spectra were collected at room temperature using a Frontier MIR/FIR Spectrometer in the ATR (Attenuated Total Reflectance) mode and using a single-point reflection GLADIATR™ diamond crystal from Pike Tech. One drop of liquid (from a Parafilm® wrapped syringe pre-

pared inside the glovebox) was placed on the diamond crystal under a flow of dry N_2 gas, to minimize the absorption of moisture by the samples during the collection time. Eight scans were acquired in the spectral range 400 to 4000 cm^{-1} with a resolution of 2 cm^{-1}. A background spectrum was also recorded and subtracted from the spectra of the ionic liquids. All spectra were normalized to the strongest recorded signal and baseline corrected.

2.3.1.3. Raman spectroscopy. Raman spectra were collected at room temperature using a InVia Reflex Raman spectrometer from Renishaw, using a 785 nm diode laser (at 10% of nominal power) as the excitation source and a diffraction grating with 1200 lines/mm. Eight scans were acquired in the spectral range 100 to 4000 cm^{-1}. Calibration was performed prior to each measurement using a Si wafer and calibrating the vibrational mode at 520.6 cm^{-1}. The ionic liquid sample was prepared inside a glovebox and placed in a custom made air-tight sample holder, designed to minimize exposure to moisture (figure S1 in the supporting information). All spectra were baseline corrected and normalized to the strongest Raman peak.

2.3.2. Quantitative analysis

2.3.2.1. Gas chromatography (GC). Samples were analyzed using a Agilent Tech. 7820A GC system with a G4513A autosampler injection system, and a Agilent Tech. J&W HP-5 GC column (30 m, 0.32 mm, 0.25 μm). The setpoint was 50 °C with a hold time of 0.5 min, two different heating curves were used, from 50 to 160 °C at a rate of 20 °C/min with a final hold time of 0.5 min and from 160 to 260 °C at a rate of 20 °C/min with a final hold time of 0.5 min. The 10 μL sample solution was injected using split mode at a ratio of 10:1. N_2 was used as a carrier, at 69 kPa. The column flow was 2.3145 mL/min. The samples, prepared in triplicates inside the glovebox, were prepared by dissolving approximately 10 mg of compound in 1.5 mL of acetonitrile. The reported GC results are the average of the triplicate values.

2.3.2.2. Water content. The analysis of the water content was performed using the Karl-Fisher (KF) titration method, using a Mettler Toledo C20S coulometric KF titrator with a Hydranal™ Coulomat AD solution. Samples were prepared inside the glovebox in a syringe (which was wrapped in Parafilm®) to avoid moisture absorption during transport from the glovebox to the KF titrator. Samples were analyzed directly after preparation.

2.3.2.3. Quantitative nuclear magnetic resonance spectroscopy (qNMR). qNMR was performed using either a Bruker Avance III 700 MHz equipped with a 5 mm QCI cryoprobe ($^1H/^{19}F/^{13}C/^{15}N$) or a Varian V NMR-S 500 MHz equipped with a 5 mm pulse field gradient dual broadband probe (^1H-$^{19}F/^{15}N$-^{31}P). All samples were prepared inside the glovebox in the same way. The balance was calibrated and checked in the same way as in the synthesis of the ionic liquids, to ensure that the masses of analyte and internal standard were as accurate as possible, since we noticed that small errors in the weighing process can result in large variations in the qNMR results. Approximately 100 mg of analyte and 100 mg of an internal standard (4-fluoroacetophenone) were measured in a small glass vial; subsequently, 0.6 mL of DMSO-d_6 was added. The vial was capped and mixed using a vortex mixer. The contents of the vial were then transferred to an NMR tube, capped and analyzed. All samples were prepared in triplicates and the qNMR results were reported as the average of the triplicate values. When using the Varian 500 MHz instrument, ^{19}F-qNMR spectra were acquired without spinning the sample, at 25 °C, with a spectral window from −60 to −120 ppm, 16 scans, 60 s of relaxation time, 30° pulse angle, 7.2 s acquisition time, $2x10^5$ points and using the predefined ^{19}F observe ^{1}H decouple pulse sequence available on the VNMRJ 4.2 software. When using the Bruker 700 MHz instrument, ^{19}F-qNMR spectra were acquired without spinning the sample, at 25 °C, with a spectral window from −60 to −120 ppm, 16 scans, 60 s of relaxation time, 90° pulse angle, 1.5 s acquisition time, $1.2x10^5$ points and using the predefined ^{19}F observe ^{1}H decouple pulse sequence available on the TOPSPIN 3.6.2 software. Spectral analysis was performed using the MestReNova 10.0.0 software. All spectra were baseline and phase corrected before peak integration. The purity calculator script was used to determine the purity assay results for the analyzed compound (the script uses the equation described in the work by Mahajan and Singh) [6].

2.3.3. Thermal analysis

2.3.3.1. Thermogravimetric analysis (TGA). TGA was carried out on a Mettler Toledo TGA/DSC 3 + equipped with an autosampler. A XS105 semi-micro balance from Mettler Toledo was used to measure all relevant masses. The ionic liquid samples were prepared in the glovebox, a small amount of liquid (around 5–8 mg) was placed in a 100 μL aluminium pan and capped with an aluminium lid with a pin hole, using a sealing press. The measurements were performed in two different ways, with and without a heating treatment. All samples were transferred from the glovebox to the autosampler carousel inside sealed containers, to avoid absorption of moisture before the start of the analyses. However, samples that did not go through the heating treatment, were placed in the carousel under N_2 flow (by following the sample pan with a N_2 gas hose) and placed inside the instrument oven as quickly as possible. On the other hand, samples that went through the drying treatment (with heat treatment samples) were simply placed on the autosampler carousel and exposed to air over a period of approximately 1 h. The non-heat treated sample method consisted in using a heating rate of 8 °C/min, an oven temperature range of 25–500 °C and N_2 flow of 60 mL/min. The heat treated sample method consisted of heating the sample at 120 °C for 30 min prior to the beginning measurement, in order to remove moisture absorbed by the ionic liquids, then the oven temperature was decreased to 25 °C and kept at this temperature for 30 min. Afterwards, the TGA experiment was performed using a heating rate of 8 °C/min, an oven temperature range of 25–500 °C and N_2 flow of 60 mL/min.

2.3.3.2. Differential scanning calorimetry (DSC). Thermal analysis by DSC was carried out using a Mettler Toledo DSC 2 equipped with an autosampler. A XS105 semi-micro balance from Mettler Toledo was used to measure all relevant masses. The ionic liquid samples were prepared in the glove box, placing a small amount of liquid (around 4–6 mg) in a 40 μL aluminium pan that was then hermetically sealed with an aluminium lid, using a sealing press. No special care was taken after removing the sealed crucibles from the glove box. The phase behavior of the liquids was investigated using two methods, the first method (slow method) consisted in two cycles of cooling and heating at the same rate of 2 °C/min, scanning over the temperature range from −100 to 60 °C, under a N_2 flow of 100 mL/min. The slow cooling was performed to promote crystal formation. In the second method (fast method), the DSC experiment consisted in three cycles, in which all the samples were cooled and then heated at the same rate of 10 °C/min. The experiment was done under N_2 flow of 100 mL/min and scanning over the temperature range from −100 to 60 °C. The rapid cooling was performed to promote glass formation and prevent crystallization. The information extracted from the second cycle in both methods is presented in the experimental section in table format (Table 2) and as a thermograph in the supporting information (figures S17-S18).

2.4. Computational methods

As a first step in the computational studies, the geometries of all ionic liquids were optimized as single ion pairs. First, 10 conformers of each ionic liquid were manually generated and optimized at the MMFF94 level of theory as implemented in the Avogadro 1.2.0 software [7]. The resulting geometries were further optimized using the PM3 level of theory as implemented in the Orca 4.1.2 software [8]. Afterwards, the two lowest energy conformers were optimized at the Hartree–Fock/6–31 + G* level of theory and then at the B3LYP-D3/6–31 + G level. Finally, the lowest energy conformation was optimized at the ωB97X-D3BJ/cc-pVTZ level of theory [9] using the RIJCOSX approximation as well as an ethanol implicit solvation model (CPCM). Numerical frequency calculations were performed in the final optimized structures; no imaginary frequencies were found, confirming that the structures were indeed in a local minimum of the potential energy surface. Molecular descriptors (electronegativity and electrophilicity) were calculated in the framework of conceptual density functional theory (CDFT) [10,11]. Simulated vibrational spectra (FTIR and Raman) were corrected (in Avogadro) using a scaling factor of 0.9542 [12]. The vibAnalysis software [13] was used to assist in the peak assignment process. The Gabedit software [14] was used to plot the electrostatic potential maps in the electronic density iso surface. All output files from Orca and vibAnalysis (with unscaled frequencies), as well as all the final optimized geometries can be found in the supporting information.

3. Results and discussion

3.1. Practical constraints

In view of the discussion of the experimental results, it is important to explain the concerns that have guided the choice of our synthesis methodology. It is well known that many ionic liquids are hygroscopic, and the fact that the water content can drastically change their properties [15] has to be taken into serious consideration during both synthesis and analysis. This concern imposes the first constraint to our experimental approach, that is designing it to always avoid exposure of the ionic liquids to atmospheric moisture. Another crucial concern is the presence of impurities. Ionic liquids are notoriously hard to purify due to their physical properties (such as low vapor pressure, low melting point and solubility), which limit the viable options for purification procedures that normally include common and effective methods like distillation, recrystallization and solvent extraction. As a consequence, the best option would be to adopt a clean synthetic procedure that involves the necessary reagents only (preferably with high purity) and avoids using solvents. This is particularly viable when synthesizing protic ionic liquids, due to the simplicity of the acid-base neutralization reaction involved. Nevertheless, one type of impurity of concern for protic ionic liquids is the excess of either acid or base, which can arise from inaccurate measurements of the amount of reagents or from transfer losses (*e.g.*, loss of material that adheres to the glassware and/or to other components of the synthesis setup). The effect of these impurities is not negligible either and is indeed the subject of vivid discussions in the literature [16].

One fundamental aim of this work has been to obtain protic ionic liquids of high purity and with an acid to base ratio as close as possible to unity, which is in practice very difficult to achieve despite the conceptual simplicity of the synthesis. In this context, the use of solvent extraction to address the issue of excess acid or base is complicated by several factors. This strategy assumes the solvent being selective (*i.e.*, removing only the targeted compound), which might not be the case with protic ionic liquids. In addition, in protic ionic liquids there is a dynamic equilibrium between charged and neutral species, due to a certain degree of back proton transfer [1]. Also, the extraction method will introduce another form of impurity, *i.e.*, solvent traces. For all these reasons, we opted for developing a truly solvent-free procedure.

An alternative strategy to deal with the excess of acid, base or solvent, is to drive them out of solution by heating under vacuum, exploiting volatility. However, heating may cause degradation of the ionic liquid by back proton transfer, shifting the final product farther from the ideal 1:1 mol ratio of acid to base. Heating is also an issue when mixing the acid and the base (which react exothermally and hence require cooling) [17], since it can cause undesired side reactions. Therefore, one additional constraint is the ionic liquid being heated as little as possible during synthesis; in this work the temperature is set to never exceed 40 °C.

Based on the concerns explained above, as many as possible of the synthesis steps (except for the acid-base neutralization reaction that requires cooling) are performed inside the glovebox. This limits the physical size of the synthesis setup and, consequently, the volume of the liquid that can be obtained for each batch. The system is also designed to be as simple as possible to enable reproducibility, an aspect that is crucial for us and can help other research groups interested in this work.

A final limitation that we have identified is the fact that the acids and the bases used in the synthesis of protic ionic liquids can be corrosive towards the materials commonly used in organic chemistry setups (*e.g.*, metals, polymers, paper, etc). Hence, all the materials supposed to come into contact with the reagents were chosen to be of glass or of chemically resistant polymers (*i.e.*, PTFE and PVDF), thus reducing the risk for further contamination.

3.2. Minimizing exposure to water

As stated above, limiting the exposure of ionic liquids to water is extremely important. Considering that to some degree, water is present in every chemical and laboratory equipment used, our presented method overcomes this difficulty as all precursors (acids and bases) were handled and stored in the glovebox, and additionally, a series of other measures with this objective were taken. HTfO is particularly problematic to work with, since it is a volatile, extremely corrosive liquid that fumes when exposed to even a minute amount of water, *i.e.*, also inside the glovebox. A recommendation is thus to purchase this acid in 25 mL ampules, and to use it as quickly as possible after opening.

Similar precautions should also be taken during any type of analysis, which most commonly occurs outside the glovebox with an inevitable exposure to water. For instance, NMR tubes were prepared inside the glovebox using dry DMSO-d_6 from ampules, Raman spectra were acquired from samples kept in a specially designed cell assembled and sealed inside the glovebox, FTIR spectra were acquired keeping the samples under a continuous flow of N_2, samples for KF titration were prepared in the glovebox (inside syringes wrapped in Parafilm M®) and pans for thermal analysis (TGA and DSC) were also prepared inside the glovebox. These procedures may sound tedious, yet we judge them necessary to ensure a correct interpretation of the collected data, such that the measured properties reflect the pure state of the liquids as stored in the glovebox.

3.3. Realizing an air- and moisture-tight synthesis setup

The synthesis setup shown in Fig. 2 was designed in light of the practical constraints discussed above, and allowed us to accomplish our goals with reasonable simplicity. As shown in Table 1, dry ionic liquids of significant purity were obtained, without the

Table 1
Purity assay and water content of the protic ionic liquids.

Protic ionic liquid	Purity assay (% m/m from ^{19}F-qNMR)	Water content (ppm)
[C_2HTr$_{124}$][TfO]	98.0	345.1
[C_2HTr$_{124}$][TFSI]	98.3	552.9
[C_2HIm][TfO][a]	99.7	bdl[b]
[C_2HIm][TFSI]	99.1	128.0

[a]From IoLiTec; [b]bdl: below detection limit.

need of solvents, vacuum distillation or other complex purification methods.

This high purity could be achieved because the synthesis setup allows for an accurate weighing and complete mixing of the precursors (further details of the weighing procedures are given in the supporting information). This limits the inclusion of excess bases or acids. The only purification method utilized after the synthesis, was the addition to the liquid of activated charcoal and molecular sieves. Activated charcoal is commonly used to remove impurities from ionic liquids [18–20], and can efficiently be filtered out after usage with PTFE syringe filters (0.2 μm). Nevertheless, it is important to point out that this kind of purification process can possibly leave trace amounts of carbon nanoparticles in the liquid phase [21]. It is thus important to consider the pros and cons of this type of purification procedure (this is also valid for other sorbents like alumina and Celite®) and always report these procedures in detail when publishing. For instance, in the case of the compounds discussed in this work, we have very limited evidence to support the use of activated charcoal, since we did not perform any thorough analysis to determine the effect of their use in the removal of trace impurities. However, we did observe (during trial synthesis of these new compounds) that triazolium ionic liquids stored in the glovebox, have a tendency to develop a slight coloration over a period of months, an effect which was reduced by using activated charcoal. Ideally, in the future, this extra purification step can be skipped (possibly by further purifying the precursors), since it also introduces the possibility of serendipitous impurities during handling of the ionic liquid. Molecular sieves are excellent for removing water from ionic liquids [22,23] but have a tendency to break into a fine powder, which must be filtered out. Although multiple and subsequent iterations can be employed to achieve extremely low levels of water content, we decided to use a single round to limit transfer losses, which are more significant in the case of small scale synthesis. Once again, it is important to balance the pros and cons of this process as well, since it can result in similar issues than the ones presented in the case of activated charcoal. In our case, we consider the use of these molecular sieves to be extremely relevant, due to the effects of moisture already discussed previously.

The synthesis setup was also successful in minimizing the exposure to atmospheric water, since it was designed to be air-tight and was kept either inside the glovebox or attached to a N_2 Schlenk line if used outside the glovebox (except for a few minutes during transfer between the glovebox and the N_2 Schlenk line). Finally, we are eager to emphasize that the system is completely modular, so that it can easily be adapted to fit other constraints such as different volumes, sizes, and materials. Also, all the parts used are commercially available (more information in the supporting information), which makes it viable and inexpensive for other research groups to mimic our methodology.

3.4. Qualitative NMR results

Essentially, the qualitative NMR analysis shows that all ionic liquids have the expected structure and have only small amounts of NMR detectable impurities. These impurities can be seen in the hydrogen and carbon NMR, but are not present in the fluorine spectra (figure S3). The ^{1}H-NMR spectra of the ionic liquids can also be used to characterize their chemical properties, most importantly, its Brønsted acidity. A useful property of solvent-free spectra is the presence of strong (N)H hydrogen peaks, whose chemical shifts have been shown to be related to their relative acidity [24]. By looking at the stack plot of the ^{1}H-NMR spectra of the ionic liquids (Fig. 3), a clear trend appears in the region 9 to 14 ppm. This trend in chemical shifts, indicates that triazolium protic ionic liquids are more acidic than imidazolium ones and that the anion also plays an effect on this character (TfO produces peaks that are further shifted downfield when compared to TFSI, and therefore result in a more acidic protic ionic liquid). This same behaviour is observed, to some extent, in the ppm region of ring hydrogens (6 to 9 ppm).

The different behaviour of triazolium and imidazolium protic ionic liquids can be rationalized by considering the electron-withdrawing effect of the extra nitrogen on the triazolium ring when compared to imidazolium (Fig. 9), which causes a deshielding of the (N)H hydrogen, pointing to an increase in acidic character. Furthermore, a similar but smaller downfield shift of the CH_2 peaks around 3.7 ppm can be observed, which further corroborates this hypothesis. The differences in acidity between TfO and TFSI protic ionic liquids can be rationalized by differences in hydrogen bonding between the cation and the different anions. The chemical shifts of the cation's (N)H and H^2 hydrogens have been hypothesized to be related to the strength of the hydrogen bonding between them and the anions [25,24]. This increased hydrogen bonding (which is the case for TfO), stretches the N-H bond, increasing its acidic character. The reverse is true for TFSI. One can think of this effect as a competition between the anion and the cation, both interested in abducting the acidic hydrogen. The stronger the hydrogen bonding is, the weaker the N-H bond will be. These effects on the downfield shifting of the peaks will be further explored in the section related to computational results. The ring carbons of triazolium are also significantly downfield shifted when compared to imidazolium, allowing us to clearly see the CF_3 quartet, which overlaps with the imidazolium ring carbon peaks (figure S2). Once again, downfield shifting can be observed, this time on the CH_2 carbon peaks of the triazolium protic ionic liquids. Finally, the fluorine spectra (figure S3) show that no other fluorinated species are present in the ionic liquids (even though only

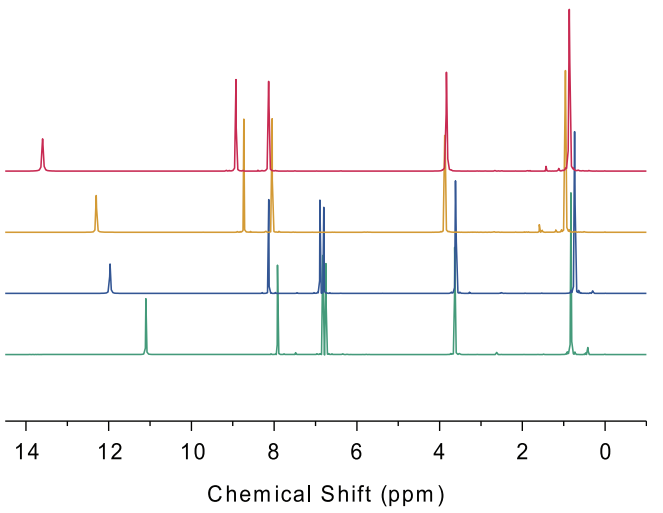

Fig. 3. ^{1}H-NMR of the ionic liquids. From the top to the bottom, [C_2HTr$_{124}$][TfO], [C_2HTr$_{124}$][TFSI], [C_2HIm][TfO] and [C_2HIm][TFSI].

a small window is presented in figure S3, no peaks within 100 ppm from the CF_3 peaks were detected) and show a small but clear distinction in the shifts of the CF_3 peaks of the TfO and TFSI anions (a difference smaller than 1 ppm).

3.5. DSC results

The DSC experiments were performed following two methods, using a slow (2 °C/min) or a fast (10 °C/min) cooling rate. Rapid cooling was chosen to prevent crystallization and promote the glass formation instead, while slow cooling was chosen to have the opposite effect. The phase behavior, *i.e.*, the temperatures of crystallization (T_c), glass transition (T_g) and melting (T_m), for all protic ionic liquids are summarized in Table 2, while the thermograms can be found in the supporting information (figure S17-S18).

It is clear that the cation has a relevant effect on the phase behaviour of the ionic liquids. Imidazolium based protic ionic liquids have a stronger tendency to form crystals, specially [C_2HIm][TfO], which always displays clear crystallization and melting peaks and no detectable glass transition, independently of the DSC method used. This tendency changes with the substitution of the anion, from TfO to TFSI, since only when using the slow method crystallization and melting events were detected. This could be due to the increased degrees of freedom of the TFSI anion, which can inhibit crystallization. In contrast, the triazolium based ionic liquids do not have a strong tendency to form crystals, and form glasses more easily. In fact, several different analysis methods were tried (not all shown here) and none resulted in crystal formation. This could be due to the reduced symmetry of the 1,2,4-triazolium ring compared to the case of imidazolium. Another possibility, is that impurities in the ionic liquids could be preventing these phase transitions from happening. This behaviour could be beneficial for certain applications that require ionic liquids with a broad window of liquid phase and no phase transitions. Another interesting observation is the presence of multiple distinct melting peaks for [C_2HIm][TfO], possibly due to the existence of multiple, energetically close crystalline configurations.

3.6. TGA results

As discussed above, when analyzing ionic liquids it is important to avoid exposure to moisture. The most common way to deal with the moisture absorbed during the TGA is to expose the sample to a heating (pre) treatment, usually consisting in heating the sample pan inside the instrument at temperatures above 100 °C for a period of tens of minutes. However, besides removing water molecules, this procedure can also result in an undesired change of the ionic liquids' composition, by means of back proton transfer and subsequent evaporation of volatile compounds. To avoid this issue, and analyze the sample in a state as close as possible to the one in storage (*i.e.*, the neat and anhydrous ionic liquid), a procedure was used that basically consists in avoiding moisture exposure at all. The results obtained in this way were compared to those obtained by running TGA in the more 'traditional' mode (Fig. 4).

The first important observation is that by utilizing the more common heat treatment a mass loss of up to 4% emerges from [C_2HTr$_{124}$][TfO] (see inset of Fig. 4b). In addition, the decomposition curve of [C_2HTr$_{124}$][TFSI] shifted towards lower temperatures. Interestingly, the heating treatment had a lesser effect on the thermographs of the imidazolium based ionic liquids. Due to these differences we recommend that, when possible, ionic liquid samples are prepared inside a glovebox and kept under N_2 flow during insertion into the TGA instrument (details in the experimental sec-

Table 2
Results from the thermal analysis by DSC of all protic ionic liquids. Values are extracted from the 2nd cycle. Multiple values indicate a set of proximate peaks.

Method	Protic ionic liquid	T_g (°C)	T_c (°C)	T_m (°C)
Fast method (10 °C/min)	[C_2HTr$_{124}$][TfO]	−65.27	-	-
	[C_2HTr$_{124}$][TFSI]	−62.60	-	-
	[C_2HIm][TfO]	-	−18.26	22.27/29.11
	[C_2HIm][TFSI]	−81.83	-	-
Slow method (2 °C/min)	[C_2HTr$_{124}$][TfO]	−67.47	-	-
	[C_2HTr$_{124}$][TFSI]	−64.31	-	-
	[C_2HIm][TfO]	-	−8.512	19.52/22.55/28.91
	[C_2HIm][TFSI]	−84.23	−47.03/-41.59	10.61

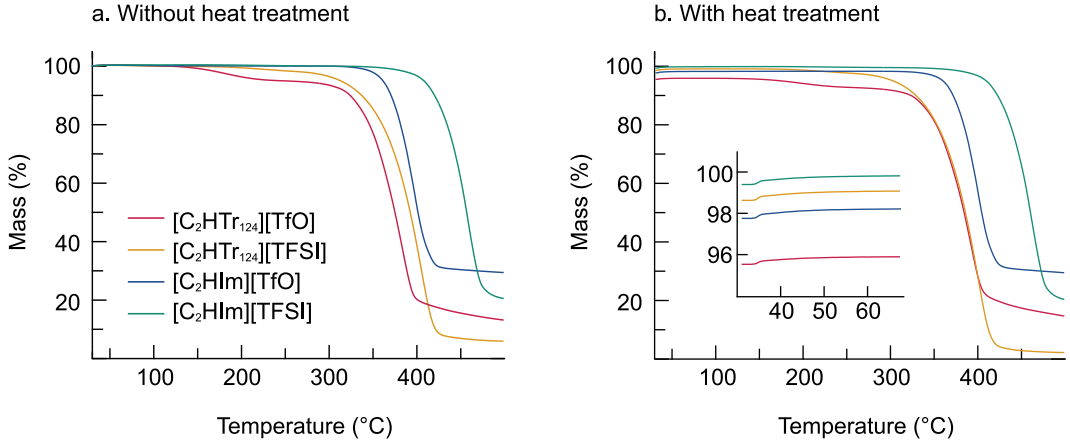

Fig. 4. Thermogravimetric curves of C_2HTr$_{124}$][TfO], [C_2HTr$_{124}$][TFSI], [C_2HIm][TfO] and [C_2HIm][TFSI] recorded under N_2 atmosphere, without (a) and with (b) a heat treatment.

tion) and that, when this is not an option, methods & results should be properly described having in mind the effects described above.

With this preamble, we can now use Fig. 4a to compare the thermal stability of the ionic liquids in this study. It is clear that triazolium ionic liquids are less stable than their imidazolium counterparts and that TfO based ionic liquids are less stable than those based on TFSI. In order to precisely determine the degradation temperature from both methods, the first derivatives of the TGA curves (d_{mass}/d_T) were plotted against temperature (Fig. 5).

It is important to point out that these curves are the result of fitting the original curves using a smoothing algorithm (original curves can be found in the supporting information, figure S16). This was done to improve the readability of the original data, which is somewhat noisy. Once again, when using the method without a pre-treatment, the lower thermal stability of the triazolium based ionic liquids becomes clear, specially for [C_2HTr_{124}][TfO] that shows two decomposition events (DTG peaks at 181 and 383 °C). The minor decomposition event at 181 °C might be related to the evaporation of HTfO, since the onset point on the TGA curve (141 °C) and the DTG peak are quite close to its boiling temperature (162 °C, as reported by the manufacturer). This might be a result of back proton transfer, which is a reasonable assumption given the fact that this ionic liquid has the most acidic (N)H among all ionic liquids in this study. This increased acidity was already discussed in the NMR section and will be further discussed in the vibrational spectroscopy and computational sections.

One could expect this first decomposition event to proceed until complete acid consumption, but that is clearly not the case. A hypothesis is that a partial evaporation of the HTfO leaves behind a more thermally stable non-stoichiometric mixture of acid and base, with an excess of base. It is possible that this same effect was responsible for the increase in thermal stability observed for compounds reported in the work of Karlsson et al. [3]. In that case, non-stoichiometric triazolium ionic liquids with low degrees of protonation (excess base) have higher thermal stabilities when compared to ionic liquids with a higher degrees of protonation (Fig. 4a from Karlsson et al.) [3]. Another important recommendation for the analysis of TGA data of protic ionic liquids is to always evaluate the thermal stability of these compounds using the thermographs, and not only the onset or DTG peak values. For example, at first sight [C_2HTr_{124}][TFSI] and [C_2HIm][TfO] might appear to be almost equally stable, since their TGA onset temperatures (357 and 369 °C respectively) and DTG peaks (405 and 398 °C respectively) are quite similar, but if we closely observe their thermographs in Fig. 4a, we can see that [C_2HTr_{124}][TFSI] starts losing mass much earlier than [C_2HIm][TfO]. A table (table S1) with DTG peak values as well as the TGA onset points for all DSC thermographs can be found in the supporting information (figures S17-S18). Further studies would be needed to properly characterize the thermal stability of these ionic liquids in more realistic conditions, such as longer periods of time at high temperatures and exposure to air, although, in general, we can state that all investigated ionic liquids are likely to be stable up to 120 °C and that a higher stability (up to 300 °C) can be achieved with the TFSI anion and the imidazolium cation.

3.7. Vibrational spectroscopy

As also described in the experimental section, and in order to reduce the influence of atmospheric moisture, all vibrational spectra were acquired keeping the sampled droplet under the flow of N_2 (FTIR) or keeping the liquid sample in a cell (figure S1) prepared in the environment of a N_2 filled glove box (Raman). This accuracy becomes specially relevant when the focus is on studying vibrational frequencies, since these can be substantially affected by the water content [26]. The simulated spectra of all ionic liquids were used to assign vibrational modes to the frequencies experimentally recorded by FTIR. However, before going through these results, the applied methodology needs to be presented and discussed.

When calculating observable properties with density functional theory (DFT) methods, a series of assumptions and approximations are made. For instance, the ideal molecular model of an ionic liquid should include as many ion pairs as necessary to account for all the inter-molecular interactions and variations in molecular conformations found in the real liquid phase. However, this would be prohibitively expensive, in terms of computational resources, while using high level DFT calculations, since such a model would be much larger than what is currently feasible (up to 200 atoms in most cases). Therefore, our model consists in a single ion pair in the gas phase and, to account for some of the solvation effects (*i.e.*, the ionic liquid solvating itself), an implicit ethanol solvation method was employed [27,28]. We found that this implicit solvation had a significant positive effect in the quality of the match between experimental and computational spectra.

Another important approximation used when calculating vibrational frequencies, is the use of a harmonic oscillator [29], where ignoring the anharmonic nature of molecular vibrations becomes another source of error. With these limitations, this technique has been, and currently is, routinely used by the computational chemistry community, and can yield excellent results. In the case

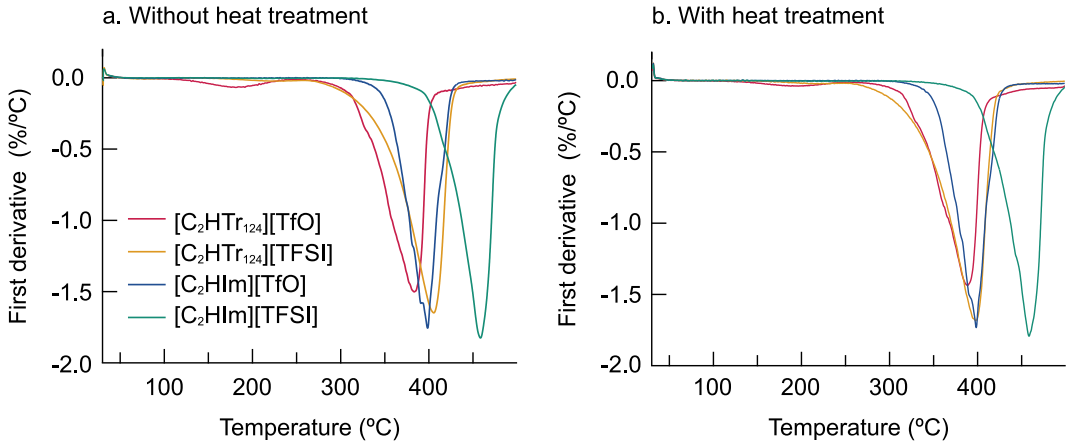

Fig. 5. Derivative thermogravimetric (DTG) curves recorded without (a) and with (b) a heat treatment.

of this work, a good match between experiments and computations was achieved (figures S5-S12).

The calculated spectra are presented in two different ways: as simple stick peak spectra (peaks with 0 peak width) and as spectra with Gaussian peaks. These two representations are relevant, since the first (stick spectra) is a more accurate representation of calculated spectra and the second (Gaussian spectra) provides a better visual correlation with the experimental spectra, which is helpful when trying to match experimental with calculated peaks. However, it is important to point out that the width of the simulated spectra in the Gaussian representation is arbitrarily chosen and has no physical meaning.

The assignment of the vibrational modes was made by comparing the spectra pair wise (experimental and calculated) and observing the animations of the respective vibrations in the Avogadro software. The vibAnalysis tool was also used to assist in this assignment process. This tool allows for a less subjective analysis of the vibrational modes, since it provides a list of all vibrational frequencies and a description of the most prominent displacements. For the sake of transparency, the Orca and vibAnalysis software output files for all ionic liquids are made available in the supporting information to the more interested reader (more precisely, the interested reader can observe and assign the vibrational mode animations using the Orca enhanced Avogadro software version available in the download section of the Orca forum) [30].

The vibrational modes that could be assigned with a reasonable level of confidence are summarized in Tables 3–6, while the atomic numbering used for the cations' assignment is illustrated in Fig. 6.

Roughly, the spectra can be divided into two regions, one from 4000 to 1400 cm^{-1} which is dominated by contributions from the cation, and another from 1400 to 400 cm^{-1} which is dominated by the vibrations of the anion. The most characteristic peaks that can be used to distinguish between the two cations, *i.e.*, imidazolium from triazolium, are present in the region from 1600 to 1500 cm^{-1} and correspond to in-plane ring stretching modes.

Distinguishing between anions is even a simpler task, since TfO and TFSI present strong, characteristic peaks in the fingerprint region, from 1400 to 1000 and from 660 to 480 cm^{-1}. For instance, the TfO ion presents a well defined, strong and isolated signal at 1024–1025 cm^{-1}, which corresponds to the symmetric stretching of SO_3. A similar vibrational mode (S-N-S asymmetric stretching with symmetric stretching of SO_2) is found for the TFSI ion peak at 1130–1131 cm^{-1}.

Interestingly, the region where the N-H stretching appears might provide additional evidence to the difference in N-H acidity (Fig. 7). In fact, the N-H stretching mode seems to shift towards lower wavenumbers in the following order, $[C_2HIm][TFSI] > [C_2HTr_{124}][TFSI] \sim [C_2HIm][TfO] > [C_2HTr_{124}][TfO]$; $[C_2HIm][TFSI]$ having the least acidic N-H group. This is however not a definitive interpretation of data, and should be considered to be inconclusive. For clarity, we choose to present the spectra as a stack of transmittance normalized (by the strongest signal at around 3150 cm^{-1}) spectra, with dashed lines indicating the positions of the calculated N-H stretching peaks, as well as providing a version of the same graph with the baselines aligned (figure S4). By visual analysis, we concluded that the shift of the N-H peak from higher to lower frequencies must be responsible for the increased area in the high frequency (2500–3500 cm^{-1}) region of $[C_2HTr_{124}][TfO]$. This shift is also suggested by the analysis of the computationally predicted vibrational frequencies (dotted lines on Fig. 7). We must add, that this kind of computational predictions should be taken with a grain of salt, since a large discrepancy between the experimental and calculated frequencies of the N-H stretching should be expected, due to the limitations of the computational method in predicting vibrational modes that are strongly influenced by their chemical environment, which is the case of the N-H stretch. Peak fitting can be used to assign specific values to vibrational modes that partly overlap, and we attempted to perform such an analysis using Voigt functions in the Fityk software [31] (figures S14-S15). However, this peak fit approach also proved to be a challenging

Table 3
Experimental FTIR and scaled calculated frequencies along with their assignment for $[C_2HTr_{124}][TfO]$.

Experimental (cm^{-1})	Calculated (cm^{-1})	Assignment[a]	Chemical moiety
3200–3000 range	2951	νN-H	Cation (ring)
3140	3155	νC^2H^*, νC^5H	Cation (ring)
2997	3032	$\nu_{as}C^6H_2^*$, $\nu_{as}C^7H_2$	Cation (alkyl chain)
2946	3013	$\nu_{as}C^7H_3^*$, νC^6H	Cation (alkyl chain)
2848	2933	$\nu_s C^7H_3$	Cation (alkyl chain)
1564	1556	In plane νRing (ν_{as}N-C^2-N)	Cation (ring)
1547	1548	In plane νRing (νC^5=N^4)	Cation (ring)
1443	1443	In plane νRing (νC^5=N^4, δN-H)	Cation (ring)
1240, 1222	1244	$\nu_{as}SO_2$	Anion (SO_3)
1158	1171	$\nu_{as}SO_2$	Anion (SO_3)
1024	990	$\nu_s SO_3$	Anion (SO_3)
967	942	νC^6-C^7	Cation (alkyl chain)
900–750 range	857	Out of plane δN-H	Cation (ring)
760	738	$\nu_s CF_3$	Anion (CF_3)
635, 625	594	$\delta_s SO_3$	Anion (SO_3)
574	553	$\delta_{as}CF_3$ and $\delta_{as}SO_3$	Anion
516	498	$\delta_{as}CF_3$ and $\delta_{as}SO_3$	Anion

[a]Abbreviations and symbols are as follows; ν: stretching; δ: bending; *s*: symmetrical; *as*: asymmetrical. *Indicates the major vibrational mode while 'and' indicates that both modes contribute with a similar intensity.

Table 4
Experimental FTIR and scaled calculated frequencies along with their assignment for $[C_2HTr_{124}][TFSI]$.

Experimental (cm^{-1})	Calculated (cm^{-1})	Assignment[a]	Chemical moiety
3200–3000 range	3199	νN-H	Cation (ring)
3152	3149	νC^2H^*, νC^5H	Cation (ring)
3000	3036	$\nu_{as}C^6H_2^*$, $\nu_{as}C^7H_2$	Cation (alkyl chain)
2956	3014	$\nu_{as}C^7H_3^*$, νC^6H	Cation (alkyl chain)
2856	2933	$\nu_s C^7H_3$	Cation (alkyl chain)
1566	1554	In plane νRing (ν_{as}N-C^2-N)	Cation (ring)
1543	1545	In plane νRing (νC^5=N^4)	Cation (ring)
1430	1427	In plane νRing (νC^5=N^4, δN-H)	Cation (ring)
1345, 1326	1293	$\nu_{as}SO_2$	Anion (SO_2)
1179	1161	$\nu_{as}CF_2$	Anion (CF_3)
1131	1104	$\nu_s SO_2^*$, ν_{as}S-N-S	Anion
1052	1030	ν_{as}S-N-S*, $\nu_s SO_2$	Anion
966	942	νC^6-C^7	Cation (alkyl chain)
900–750 range	800	Out of plane δN-H	Cation (ring)
791	774	ν_sS-N-S	Anion
742	724	ν_sS-N-S*, $\nu_s CF_3$	Anion
611, 599	578	$\delta_s SO_2$	Anion (SO_2)
570	547	δCF_2 and δSO_2	Anion
509	488	δCF_2 and δSO_2	Anion
409	381	δN-S = O	Anion

[a]Abbreviations and symbols are as follows; ν: stretching; δ: bending; *s*: symmetrical; *as*: asymmetrical. *Indicates the major vibrational mode while 'and' indicates that both modes contribute with a similar intensity

Table 5
Experimental FTIR and scaled calculated frequencies along with their assignment for [C_2HIm][TfO].

Experimental (cm^{-1})	Calculated (cm^{-1})	Assignment[a]	Chemical moiety
3200–3000 range	3083	νN-H	Cation (ring)
3149	3155	νC^2H^*, $\nu_{as}C^{4,5}H$	Cation (ring)
3115	3146	$\nu_{as}C^{4,5}H$	Cation (ring)
3021	3030	$\nu_{as}C^6H_2^*$, $\nu_{as}C^7H_2$	Cation (alkyl chain)
2988	3008	$\nu_{as}C^7H_3^*$, $\nu_sC^6H_2$	Cation (alkyl chain)
2952	2975	$\nu_sC^6H_2$	Cation (alkyl chain)
2889	2928	$\nu_sC^7H_3$	Cation (alkyl chain)
1582	1575	In plane νRing (νC^4=C^5)	Cation (ring)
1550	1534	In plane νRing (ν_{as}N-C^2-N)	Cation (ring)
1471	1456	In plane νRing (νC^4=C^5, δN-H)	Cation (ring)
1453	1440	$\delta_sC^6H_2^*$, $\delta_sC^7H_2$	Cation (alkyl chain)
1239, 1223	1239	$\nu_{as}SO_2$	Anion (SO_3)
1155	1178	$\nu_{as}SO_2$	Anion (SO_3)
1025	992	ν_sSO_3	Anion (SO_3)
960	936	νC^6-C^7	Cation (alkyl chain)
900–750 range	819	Out of plane δN-H	Cation (ring)
757	737	ν_sCF_3	Anion (CF_3)
635, 622	595	δ_sSO_3	Anion (SO_3)
573	552	$\delta_{as}CF_3$ and $\delta_{as}SO_3$	Anion
516	497	$\delta_{as}CF_3$ and $\delta_{as}SO_3$	Anion

[a]Abbreviations and symbols are as follows; ν: stretching; δ: bending; *s*: symmetrical; *as*: asymmetrical. *Indicates the major vibrational mode while 'and' indicates that both modes contribute with a similar intensity

Table 6
Experimental FTIR and scaled calculated frequencies along with their assignment for [C_2HIm][TFSI].

Experimental (cm^{-1})	Calculated (cm^{-1})	Assignment[a]	Chemical moiety
3271	3300	νN-H	Cation (ring)
3161	3162	νC^2H^*, $\nu_sC^{4,5}H$	Cation (ring)
3118	3148	$\nu_{as}C^{4,5}H$	Cation (ring)
3018	3028	$\nu_{as}C^6H_2^*$, $\nu_{as}C^7H_2$	Cation (alkyl chain)
2993	3009	$\nu_{as}C^7H_3^*$, $\nu_sC^6H_2$	Cation (alkyl chain)
2953	2973	$\nu_sC^6H_2$	Cation (alkyl chain)
2890	2929	$\nu_sC^7H_3$	Cation (alkyl chain)
1581	1572	In plane νRing (νC^4=C^5)	Cation (ring)
1550	1535	In plane νRing (ν_{as}N-C^2-N)	Cation (ring)
1472	1443	In plane νRing (νC^4=C^5, δN-H)	Cation (ring)
1451	1439	$\delta_sC^6H_2^*$, $\delta_sC^7H_2$	Cation (alkyl chain)
1346, 1329	1291	$\nu_{as}SO_2$	Anion (SO_2)
1179	1159	$\nu_{as}CF_2$	Anion (CF_3)
1130	1104	$\nu_sSO_2^*$, ν_{as}S-N-S	Anion
1052	1031	ν_{as}S-N-S*, ν_sSO_2	Anion
960	934	νC^6-C^7	Cation (alkyl chain)
900–750 range	791	Out of plane δN-H	Cation (ring)
790	769	ν_sS-N-S	Anion
740	722	ν_sS-N-S and ν_sCF_3	Anion
610, 599	579	δSO_2	Anion (SO_2)
569	546	δCF_2 and δSO_2	Anion
509	487	δCF_2 and δSO_2	Anion
410	378	δN-S = O	Anion

[a]Abbreviations and symbols are as follows; ν: stretching; δ: bending; *s*: symmetrical; *as*: asymmetrical. *Indicates the major vibrational mode while 'and' indicates that both modes contribute with a similar intensity

task, resulting in a different order than the one assigned by visual inspection (or the one indicated by Fig. 3). More details on the fitting procedure can be found in the supporting information. Overall, we believe that the only firm conclusion that can be drawn from this data is that [C_2HIm][TFSI] is significantly different from the other three protic ionic liquids, confirming a difference between the acidic character of triazolium and imidazolium protic ionic liquids. The same conclusion cannot be drawn from [C_2HTr_{124}][TfO], since its N-H mode is very broad and of low intensity.

Additionally, there is some evidence that information about the chemical environment of the N-H bond can also be extracted from the region from 900 to 750 cm^{-1}, where theory predicts the existence of an out of plane N-H bending mode. However, the precise assignment of such vibrations to specific frequencies observed experimentally was not possible in this work.

Even though the fingerprint region is dominated by anion signals, the region from 1000 to 900 cm^{-1} can be used to distinguish between cations, however the only peaks we could assign with confidence were the νC^6-C^7 stretch peaks, which are shifted by 6–7 cm^{-1} due to the different electronic environments of the two cation rings.

Regarding the TFSI anion, it is well known that it can be present in the liquid phase of an ionic liquid as an equilibrium between two conformers, the *cisoid* and the *transoid*, the latter being the conformer of lowest energy [32]. The coexistence of the two arises from the very low energy difference, which is in the order of 3–7 kJ/mol [33]. In the protic ionic liquids at focus in this work, *i.e.*, [C_2HIm][TFSI] and [C_2HTr_{124}][TFSI], the presence of both conformers is evidenced in the low-frequency region of the Raman spectrum, *i.e.*, in the 350 to 270 cm^{-1} range where the peak at 327 cm^{-1} exclusively characteristic of the *cisoid* [34] appears,

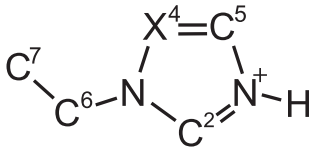

Fig. 6. Atomic numbering of the cations' structures used for the assignment of vibrational modes. The atom labelled X^4 can be either carbon (imidazolium cation) or nitrogen (triazolium cation).

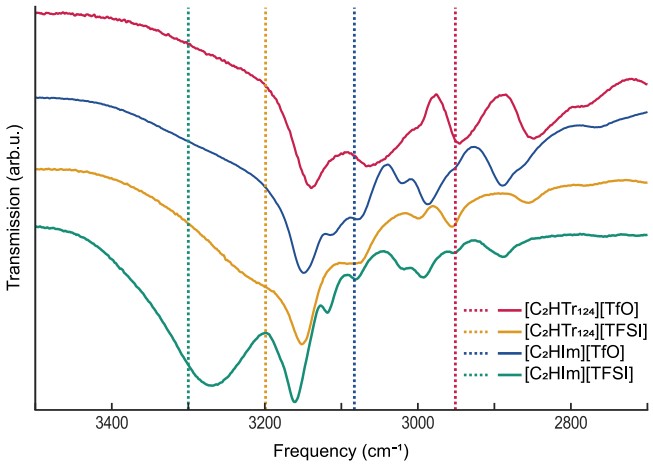

Fig. 7. Experimentally recorded FTIR spectra, of all four ionic liquids, in the frequency region of the N-H stretching mode. Dashed lines correspond to the calculated frequencies for the N-H stretching.

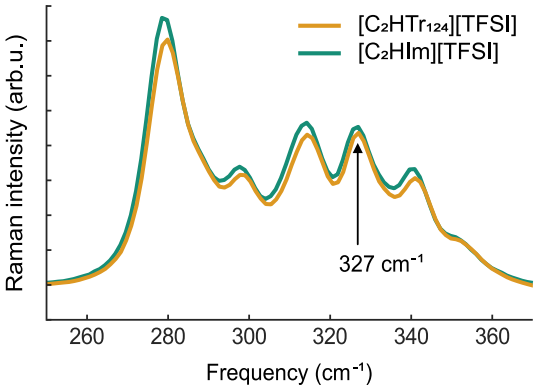

Fig. 8. Experimentally recorded Raman spectra of $[C_2HTr_{124}][TFSI]$ and $[C_2HIm][TFSI]$ in the spectral range from 350 to 270 cm^{-1}.

while the rest of the spectral shape is a combination of peaks arising from both the *cisoid* and the *transoid* conformers (Fig. 8). The Raman spectra in the entire recorded spectral range, for all ionic liquids, are available in the supporting information (Figure S13).

3.8. Computational results

Two important steps in any DFT calculation are the choice of level of theory and of molecular geometry. In this work, the dispersion corrected [35] ωB97X-D3BJ functional was chosen due to its great performance in a variety of calculations against the GMTKN55 database [9], which was also used in the excellent benchmark study by Goerigk et al. [36]. Here, it is important to recall that the D3BJ correction is essential to accurately describe dispersion effects, which are specially relevant when studying ionic liquids [37]. With respect to the geometry, it is well known that ionic liquids have relatively smooth potential energy surfaces (*i.e.*, can adopt several different conformations with small energy differences), therefore, choosing an optimized conformation to perform the calculations is not a trivial task. When performing calculations with a single ion pair, one should always aim to find its lowest energy conformation, since it will better represent the behaviour of the real bulk compound. In this work, this was done manually (as described in the experimental section); however, tools developed by Grimme's group like the CREST [38] and CENSO software [39] can be extremely useful, since they offer the opportunity to more thoroughly explore the molecular conformational space.

We already discussed the use of DFT to predict vibrational spectra but, that aside, this type of calculations can also be used to achieve useful information about the electronic structure of molecules through the framework of CDFT [10,11]. Using this framework, molecular descriptors (*i.e.* numerical representations of molecular properties) could be calculated and were in fact used to compare the relative acidity of the four protic ionic liquids. In this study, two CDFT descriptors (electronegativity and electrophilicity) were considered, as well as the optimized bond lengths and the partial atomic charges using the CHELPG scheme [40].

These CDFT descriptors (Table 7) are well described in the literature [10,11] and provide a quantitative measure of the tendency of a molecule to act as an acceptor of electrons (Lewis acid). Our assumption is that both the Lewis and the Brønsted acidity are affected by the electronic configuration in a similar way, hence and in general a strong Brønsted acid should also be a strong Lewis acid. This has been shown to be a plausible hypothesis in a previous work by Gupta et al. [41].

Table 7
CDFT molecular descriptors for all the optimized ionic liquid ion pairs in the ωB97X-D3BJ/cc-pVTZ level of theory.

Protic ionic liquid	Eletronegativity (eV)	Electrophilicity (eV)
$[C_2HTr_{124}][TfO]$	4.5839	1.7482
$[C_2HTr_{124}][TFSI]$	4.8269	1.8888
$[C_2HIm][TfO]$	4.1659	1.4525
$[C_2HIm][TFSI]$	4.2305	1.5052

The CDFT descriptors found here clearly show that the triazolium based protic ionic liquids are more acidic (higher electronegativity and electrophilicity) and that the anion has a significantly smaller effect on these electronic properties. This difference in electronic structure between the two cations, is exemplified by comparing the electrostatic potential map of $[C_2HTr_{124}][TfO]$ and $[C_2HIm][TfO]$, Fig. 9.

There is a clear redistribution of the electrostatic potential in the cations due to the electron withdrawing effect of the unsubstituted nitrogen in the triazolium ring. This is most likely the main reason for the increase in the acidity of the triazolium protic ionic liquids when compared to the imidazolium counterparts. The increase in the N-H bond length is yet another piece of evidence for this increase in acidity (Table 8).

The lengthening of the N-H bond follows an order that is somewhat compatible with the FTIR and NMR results for this chemical moiety, with the compound $[C_2HTr_{124}][TfO]$ having the longest bond and $[C_2HIm][TFSI]$ having the shortest. Considering the intermolecular interactions between both ions, the interatomic lengths seem to indicate that the triazolium ring increases the intermolecular interactions (shorter $(N)H\cdots O^{anion}$ and $N(H)\cdots O^{anion}$ interatomic lengths) when compared to the imidazolium ring. It is also apparent that the TfO anion has stronger interactions with the cations when compared to TFSI, as evidenced by shorter hydrogen bond distances ($(N)H\cdots O^{anion}$). These results point once again to the general conclusion that triazolium protic ionic liquids are more acidic than their imidazolium counterparts, and that TfO based protic ionic liquids will also result in more acidic compounds than those based on TFSI. Nevertheless, it is important to point out that, as for all other results from this computational study, there is a dependency on the choice of molecular models. In other words, if other conformers (or even using molecular clusters instead of single ion pairs) had been used to calculate these descriptors, slightly different descriptor values (bond lenghts, charges, electronegativity and electrophilicity) would have been expected. We believe that these differences would not significantly change the general conclusions stated previously, but that is a matter that still has to be evaluated more thoroughly, since is outside of the scope of this work. Finally we look at partial atomic charges (Fig. 10).

The difference between the partial atomic charges of the H and N atoms in the N-H moiety of the cations can be used as a measure of bond charge polarization, which is a classic indicator of Brønsted acidity. Once again, the same trend is observed in regards to ordering, with $[C_2HTr_{124}][TfO]$ having the largest difference and $[C_2HIm][TFSI]$ the smallest. This once again points to a higher acidic character of the triazolium based protic ionic liquids, in particular $[C_2HTr_{124}][TfO]$. Additionally, it is important to point out that, although very popular and widely used for this type of analysis, the CHELPG scheme is outperformed by other charge schemes, as discussed in the work by Rigby and Izgorodina [42]. This does not necessarily mean that CHELPG is not suitable for this sort of analysis since it has even been shown, in a combined computational and experimental X-ray study, to be a good descriptor of molecular charge distribution in ionic liquids [43].

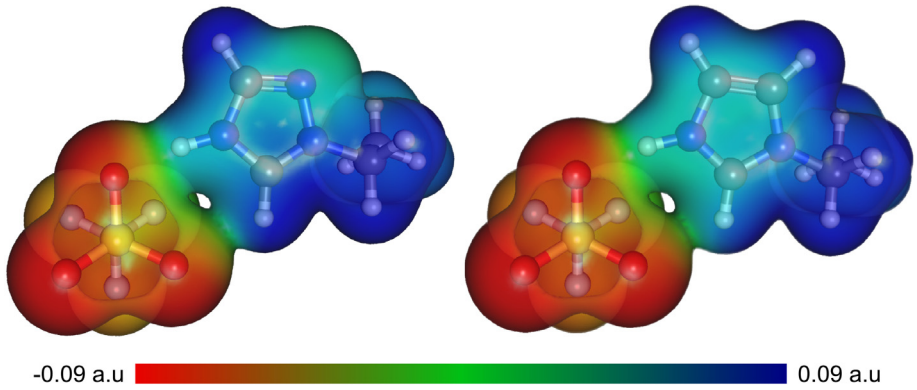

Fig. 9. Electrostatic potential map (plotted on the electron density iso surface with a value of 0.007) for the $[C_2HTr_{124}][TfO]$ and $[C_2HIm][TfO]$ optimized ion pairs in the ωB97X-D3BJ/cc-pVTZ level of theory.

Table 8
Selected bonds and interatomic lengths (Å) for all the optimized ionic liquid ion pairs in the ωB97X-D3BJ/cc-pVTZ level of theory.

Protic ionic liquid	N-H	$(N)H\cdots O^{anion}$	$N(H)\cdots O^{anion}$
$[C_2HTr_{124}][TfO]$	1.038	1.708	2.738
$[C_2HTr_{124}][TFSI]$	1.025	1.858	2.882
$[C_2HIm][TfO]$	1.031	1.763	2.787
$[C_2HIm][TFSI]$	1.019	1.950	2.959

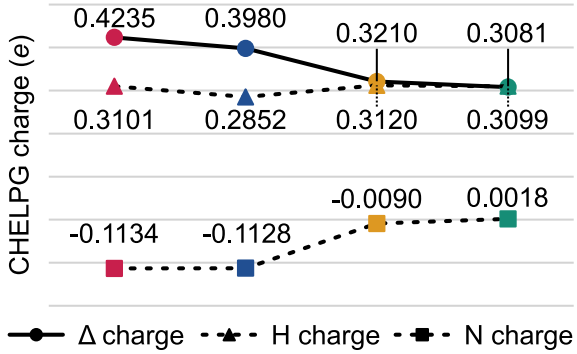

Fig. 10. Partial atomic charges (CHELPG scheme) for all the optimized ionic liquid ion pairs in the ωB97X-D3BJ/cc-pVTZ level of theory. From left to right respectively: $[C_2HTr_{124}][TfO]$, $[C_2HIm][TfO]$, $[C_2HTr_{124}][TFSI]$ and $[C_2HIm][TFSI]$.

4. Conclusions

The methods described in this work allow for the laboratory-scale solvent-free synthesis and characterization of protic ionic liquids with reasonably high purity and low water content. This was achieved keeping the complexity of the procedure as low as possible. Nevertheless, we expect that with the help of the ionic liquid community we will be able to further simplify the process without compromising the quality of the products, making it even more accessible to a broader span of researchers. The characterization presented here indicates clear differences between the investigated ionic liquids; those based on triazolium having a lower thermal stability but a higher acidity, and *vice versa* for the ionic liquids based on imidazolium. The anion also has a clear effect in the observed properties; i.e., the ionic liquids based on TfO display a lower thermal stability and a higher acidity, while the TFSI based ionic liquids show the opposite trend. The analysis of the acidity of these compounds was possible due to the use of DFT techniques in conjunction with spectroscopic methods (NMR and FTIR), which were also used to assign vibrational modes to the experimental FTIR spectra.

Declaration of Competing Interest

The authors declare that they have no known competing financial interests or personal relationships that could have appeared to influence the work reported in this paper.

Acknowledgement

Funding support from the Knut and Alice Wallenberg Foundation (Wallenberg Academy Fellows, grant 2016–0220) and the Swedish Research Council (VR, 2018, Grant No. 05207) is kindly acknowledged. The computations were performed on resources provided by the Swedish National Infrastructure for Computing (SNIC) at HPC2N, C3SE and NSC. We would like to thank the Swedish NMR Center in Gothenburg for the allocated spectrometer time. The gas chromatography analysis was possible due to the help of August Runemark and Prof. Henrik Sundén. Finally, we want to express our gratitude to Dr. Mohammad Hasani for designing the air-tight Raman cell and the Chalmers Mechanics Workshop for manufacturing it.

Appendix A. Supplementary material

Supplementary data associated with this article can be found, in the online version, at https://doi.org/10.1016/j.molliq.2022.119358.

References

[1] T.L. Greaves, C.J. Drummond, Protic ionic liquids: Evolving structure–property relationships and expanding applications, Chem. Rev. 115 (2015) 11379–11448.
[2] D.R. MacFarlane, N. Tachikawa, M. Forsyth, J.M. Pringle, P.C. Howlett, G.D. Elliott, J.H. Davis, M. Watanabe, P. Simon, C.A. Angell, Energy applications of ionic liquids, Energy Environ. Sci. 7 (2014) 232–250.
[3] C. Karlsson, C. Strietzel, H. Huang, M. Sjödin, P. Jannasch, Nonstoichiometric triazolium protic ionic liquids for all-organic batteries, ACS Applied Energy Materials 1 (2018) 6451–6462.
[4] J. Luo, J. Hu, W. Saak, R. Beckhaus, G. Wittstock, I.F.J. Vankelecom, C. Agert, O. Conrad, Protic ionic liquid and ionic melts prepared from methanesulfonic acid and 1H–1,2,4-triazole as high temperature PEMFC electrolytes, J. Mater. Chem. 21 (2011) 10426–10436.
[5] T. Alpers, T.W.T. Muesmann, O. Temme, J. Christoffers, Perfluorinated 1,2,3- and 1,2,4-triazolium ionic liquids, Eur. J. Org. Chem. 2018 (2018) 4331–4337.
[6] S. Mahajan, I.P. Singh, Determining and reporting purity of organic molecules: why qNMR, Magn. Reson. Chem. 51 (2013) 76–81.
[7] M.D. Hanwell, D.E. Curtis, D.C. Lonie, T. Vandermeersch, E. Zurek, G.R. Hutchison, Avogadro: an advanced semantic chemical editor, visualization, and analysis platform, Journal of Cheminformatics 4 (2012).

[8] F. Neese, The ORCA program system, WIREs Computational Molecular, Science 2 (2012) 73–78.
[9] A. Najibi, L. Goerigk, The nonlocal kernel in van der Waals density functionals as an additive correction: An extensive analysis with special emphasis on the B97M-V and ωB97M-V approaches, J. Chem. Theory Comput. 14 (2018) 5725–5738.
[10] P. Geerlings, F. De Proft, W. Langenaeker, Conceptual density functional theory, Chem. Rev. 103 (2003) 1793–1874.
[11] P.K. Chattaraj, S. Giri, S. Duley, Update 2 of: Electrophilicity index, Chemical Reviews 111 (2011) PR43–PR75.
[12] M.K. Kesharwani, B. Brauer, J.M.L. Martin, Frequency and zero-point vibrational energy scale factors for double-hybrid density functionals (and other selected methods): Can anharmonic force fields be avoided?, The Journal of Physical Chemistry A 119 (2015) 1701–1714
[13] F. Teixeira, M.N.D.S. Cordeiro, Improving vibrational mode interpretation using bayesian regression, J. Chem. Theory Comput. 15 (2019) 456–470.
[14] A.-R. Allouche, Gabedit—a graphical user interface for computational chemistry softwares, J. Comput. Chem. 32 (2011) 174–182.
[15] N. Yaghini, J. Pitawala, A. Matic, A. Martinelli, Effect of water on the local structure and phase behavior of imidazolium-based protic ionic liquids, J. Phys. Chem. B 119 (2015) 1611–1622.
[16] D.E. Smith, D.A. Walsh, The nature of proton shuttling in protic ionic liquid fuel cells, Advanced Energy Materials 9 (2019) 1900744.
[17] G.L. Burrell, I.M. Burgar, F. Separovic, N.F. Dunlop, Preparation of protic ionic liquids with minimal water content and 15N NMR study of proton transfer, Phys. Chem. Chem. Phys. 12 (2010) 1571–1577.
[18] G.B. Appetecchi, S. Scaccia, C. Tizzani, F. Alessandrini, S. Passerini, Synthesis of hydrophobic ionic liquids for electrochemical applications, Journal of The Electrochemical Society 153 (2006) A1685.
[19] P. Nockemann, K. Binnemans, K. Driesen, Purification of imidazolium ionic liquids for spectroscopic applications, Chem. Phys. Lett. 415 (2005) 131–136.
[20] B. Clare, A. Sirwardana, D.R. MacFarlane, Synthesis, Purification and Characterization of Ionic Liquids, Springer, Berlin Heidelberg, Berlin, Heidelberg, 2010, pp. 1–40.
[21] B.R. Clare, P.M. Bayley, A.S. Best, M. Forsyth, D.R. MacFarlane, Purification or contamination? the effect of sorbents on ionic liquids, Chem. Commun. 2689–2691 (2008).
[22] D.B.G. Williams, M. Lawton, Drying of organic solvents: Quantitative evaluation of the efficiency of several desiccants, The Journal of Organic Chemistry 75 (2010) 8351–8354.
[23] M. Gnahm, D.M. Kolb, The purification of an ionic liquid, J. Electroanal. Chem. 651 (2011) 250–252.
[24] S.K. Davidowski, F. Thompson, W. Huang, M. Hasani, S.A. Amin, C.A. Angell, J.L. Yarger, Nmr characterization of ionicity and transport properties for a series of diethylmethylamine based protic ionic liquids, J. Phys. Chem. B 120 (2016) 4279–4285, PMID: 27088704.
[25] T. Cremer, C. Kolbeck, K. Lovelock, N. Paape, R. Wölfel, P. Schulz, P. Wasserscheid, H. Weber, J. Thar, B. Kirchner, F. Maier, H.-P. Steinrück, Towards a molecular understanding of cation–anion interactions—probing the electronic structure of imidazolium ionic liquids by nmr spectroscopy, x-ray photoelectron spectroscopy and theoretical calculations, Chemistry – A, European Journal 16 (2010) 9018–9033.
[26] V.H. Paschoal, L.F.O. Faria, M.C.C. Ribeiro, Vibrational spectroscopy of ionic liquids, Chem. Rev. 117 (2017) 7053–7112.
[27] S. Chen, E.I. Izgorodina, Prediction of 1H NMR chemical shifts for clusters of imidazolium-based ionic liquids, Phys. Chem. Chem. Phys. 19 (2017) 17411–17425.
[28] K. Low, S.Y.S. Tan, E.I. Izgorodina, An ab initio study of the structure and energetics of hydrogen bonding in ionic liquids, Frontiers in Chemistry 7 (2019) 208.
[29] S. Grimme, Supramolecular binding thermodynamics by dispersion-corrected density functional theory, Chemistry – A, European Journal 18 (2012) 9955–9964.
[30] Orca software forum, 2021. URL: https://orcaforum.kofo.mpg.de/.
[31] M. Wojdyr, Fityk: a general-purpose peak fitting program, J. Appl. Crystallogr. 43 (2010) 1126–1128.
[32] M. Herstedt, M. Smirnov, P. Johansson, M. Chami, J. Grondin, L. Servant, J.C. Lassègues, Spectroscopic characterization of the conformational states of the bis(trifluoromethanesulfonyl)imide anion (TFSI), J. Raman Spectrosc. 36 (2005) 762–770.
[33] A. Martinelli, A. Matic, P. Johansson, P. Jacobsson, L. Börjesson, A. Fernicola, S. Panero, B. Scrosati, H. Ohno, Conformational evolution of TFSI in protic and aprotic ionic liquids, J. Raman Spectrosc. 42 (2011) 522–528.
[34] A. Martinelli, Conformational changes and phase behaviour in the protic ionic liquid 1-ethylimidazolium bis(trifluoromethylsulfonyl)imide in the bulk and nano-confined state, Eur. J. Inorg. Chem. 2015 (2015) 1300–1308.
[35] S. Grimme, S. Ehrlich, L. Goerigk, Effect of the damping function in dispersion corrected density functional theory, J. Comput. Chem. 32 (2011) 1456–1465.
[36] L. Goerigk, A. Hansen, C. Bauer, S. Ehrlich, A. Najibi, S. Grimme, A look at the density functional theory zoo with the advanced GMTKN55 database for general main group thermochemistry, kinetics and noncovalent interactions, Phys. Chem. Chem. Phys. 19 (2017) 32184–32215.
[37] Z.L. Seeger, E.I. Izgorodina, A systematic study of DFT performance for geometry optimizations of ionic liquid clusters, J. Chem. Theory Comput. 16 (2020) 6735–6753.
[38] P. Pracht, F. Bohle, S. Grimme, Automated exploration of the low-energy chemical space with fast quantum chemical methods, Phys. Chem. Chem. Phys. 22 (2020) 7169–7192.
[39] S. Grimme, F. Bohle, A. Hansen, P. Pracht, S. Spicher, M. Stahn, Efficient quantum chemical calculation of structure ensembles and free energies for nonrigid molecules, The Journal of Physical Chemistry A 125 (2021) 4039–4054.
[40] C.M. Breneman, K.B. Wiberg, Determining atom-centered monopoles from molecular electrostatic potentials. the need for high sampling density in formamide conformational analysis, J. Comput. Chem. 11 (1990) 361–373.
[41] K. Gupta, D. Roy, V. Subramanian, P. Chattaraj, Are strong Brønsted acids necessarily strong lewis acids?, J Mol. Struct. (Thoechem) 812 (2007) 13–24.
[42] J. Rigby, E.I. Izgorodina, Assessment of atomic partial charge schemes for polarisation and charge transfer effects in ionic liquids, Phys. Chem. Chem. Phys. 15 (2013) 1632–1646.
[43] R.M. Fogarty, R.P. Matthews, C.R. Ashworth, A. Brandt-Talbot, R.G. Palgrave, R. A. Bourne, T. Vander Hoogerstraete, P.A. Hunt, K.R.J. Lovelock, Experimental validation of calculated atomic charges in ionic liquids, J. Chem. Phys. 148 (2018) 193817.